Data supplement for Garrison et al., Transdiagnostic Connectome-Based Prediction of Craving. Am J Psychiatry (doi: 10.1176/appi.ajp.21121207)

Supplementary Methods

Participants

Data were included from several prior studies (1-6) utilizing a personalized guided imagery task during fMRI. Other than alcohol and cocaine use disorder subgroups, no other participants met criteria for current Axis I disorder including substance use disorders. Adult controls included a subgroup of social drinkers used for comparison in the earlier study of alcohol use disorder. Of the sample, 52% were White, 37% were Black or African American, 4% were Asian, 4% were biracial, 1% were other race, and 2% were unknown race. All participants were free of significant neurological or psychiatric disorders or medical conditions. Additional exclusion criteria included inability to read and write in English, use of psychotropic medications, history of head trauma, pregnancy, claustrophobia or metal in body incompatible with MRI. For more detailed participant characteristics, see the original reports (1-6).

Personalized guided imagery paradigm

During fMRI, participants were presented with six personalized guided imagery scripts: two appetitive, two stress, and two neutral-relaxing. For the appetitive condition, in the substance use-related group, individuals with alcohol use disorder were presented with alcohol cue scripts, those with cocaine use disorder were presented with

cocaine cue scripts, and those with obesity or prenatal cocaine exposure were presented with favorite-food cue scripts. In the control group, adult social drinkers were presented with alcohol cue scripts, and all other controls were presented with favorite-food cue scripts. Standardized structured interviews were conducted using the Scene Development Questionnaire (7) to develop personally tailored scripts (7-9). Appetitive scripts were based on participants' experiences of substance (i.e., drug, alcohol, food) anticipation and consumption (e.g., birthday celebration, meeting friends at a bar; pizza, ice cream). Stress scripts were based on experiences that made them "sad, mad or upset in that moment and they could do nothing to change it" (e.g., death in the family, romantic break-up). Appetitive and stress scripts were calibrated to ensure equivalent emotional valence across participants. Neutral-relaxing scripts were based on experiences of neutral or relaxing situations (e.g., sitting in the park).

Imagery scripts were presented in a blocked design with 5.5min blocks, each comprised of a 1.5min baseline, followed by a 2.5min imagery script, and a 1min recovery. During baseline, participants were instructed to lay still and not do anything. During recovery, they were instructed to stop imagining and lay still for another minute. The order of imagery conditions was randomized and counterbalanced, with no condition repeated consecutively, and each script presented only once. Following each block, participants took part in 2min of progressive relaxation, where they were instructed to relax muscles in each part of the body (i.e., to relax physiological muscle tension rather than mental relaxation).

Before and after each imagery script, participants rated their craving (as described in the manuscript) and anxiety on verbal analog scales from 1 "not at all" to

10 “more than ever” or “extremely high.” Anxiety ratings indicated how “tense, anxious and/or jittery” they felt. Participants also rated imagery vividness by indicating how well they were able to visualize each of their individual scripts. Heart rate was monitored during fMRI using a pulse oximeter. Each subsequent imagery block began only once participants’ heart rate and subjective ratings had returned to baseline.

All images were collected at the Yale Magnetic Resonance Research Center using a 3T Siemens Trio MRI system. Participants in studies with food cues were asked to eat ~2h prior to scanning so that they were neither too full nor hungry (1, 2, 7). Individuals with cocaine use disorder were abstinent for at least 2 weeks prior to scanning (3). All participants were asked not to consume alcohol for 72h prior to scanning (4) and those with alcohol use disorder had been abstinent for 4-8 weeks (5).

Image acquisition

All images were collected at the Yale Magnetic Resonance Research Center using a 3T Siemens Trio MRI system equipped with a standard quadrature head coil. Images were acquired as follows, except where noted in the original manuscripts (1-6). Functional images were acquired using a single-shot gradient echo-planar imaging sequence (EPI) with 32 axial slices parallel to the AC-PC line covering the whole brain (TR = 2000 ms, TE = 25 ms, bandwidth = 2005 Hz/pixel, flip angle = 85°, FOV = 220 × 220 mm, matrix = 64 × 64, 32 slices with slice thickness = 4 mm and no gap, 150 measurements. Anatomical images of slice locations were acquired using a spin-echo sequence in the axial plane parallel to the AC-PC line with TR = 300 msec, TE = 2.46 msec, bandwidth = 310 Hz/pixel, flip angle = 60°, field of view = 220 x 220 mm, matrix = 256 x 256, 32 slices with slice thickness = 4mm and no gap. Anatomical images were

acquired using a sagittal high-resolution T1-weighted 3D magnetization-prepared-rapid-gradient-echo (MPRAGE) sequence with TR = 2530 ms; TE = 3.34 ms; bandwidth = 180 Hz/pixel; flip angle = 7°; slice thickness = 1mm; field-of-view = 256 × 256 mm; matrix = 256 x 256).

Connectivity processing

Functional images were motion corrected using SPM12. All further analyses were performed using BioImage Suite (8) unless otherwise specified. Several covariates of no interest were regressed from the data including linear and quadratic drifts, mean cerebral-spinal-fluid (CSF) signal, mean white-matter signal, and mean gray matter signal. For additional control of possible motion-related confounds, a 24-parameter motion model (including six rigid-body motion parameters, six temporal derivatives, and these terms squared) was regressed from the data. The data were temporally smoothed with a Gaussian filter (approximate cutoff frequency=0.12Hz).

Construction of connectomes

Nodes were defined using the Shen 268-node brain atlas, which includes the cortex, subcortex, and cerebellum as described in prior CPM work (9). If a node was missing from any individual due to incomplete brain coverage, we excluded that node from the analysis. In total, twenty-one nodes located in the brain stem, inferior cerebellum, temporal pole, and inferior orbital frontal lobe (Figure S1) were removed from analysis. These nodes were primarily in the cerebellum and brain stem. The atlas was warped from MNI space into single-subject space via series of linear and non-linear transformations (10). Task connectivity was calculated on the basis of the ‘raw’ task time courses, with no regression of task-evoked activity, which emphasizes individual

differences in connectivity. This involved computation of the mean time courses for each of the 268 nodes (i.e., averaging the time courses of all constituent voxels). Node-by-node pairwise correlations were computed, and Pearson correlation coefficients were Fisher z-transformed to yield symmetric 268x268 connectivity matrices, in which each element of the matrix represents the connectivity strength between two individual nodes (i.e., 'edge').

Assessing prediction performance

As described in brief in the manuscript, for the 10-fold cross-validation analyses, model performance was evaluated with a cross-validated coefficient of determination, labeled q^2: $q^2 = 1 - \frac{\sum_{i=1}^{n}(y_i - \hat{y}_i)^2}{\sum_{i=1}^{n}(y_i - \overline{y})^2}$, where y_i is the i^{th} observed value, $\hat{y}_i$ is the i^{th} predicted value, and $\overline{y}$ is the average of observed values. In the text, the median q^2 for 100 random 10-fold divisions is reported. For convenience, Pearson's correlation (r), Spearman's rank correlation (ρ), and mean square error (MSE; defined as: $MSE = \sqrt{(1/n \sum_{\{i=1\}}^{n}(y_i - \hat{y}_i)^2)}$ are also reported. To assess significance of q^2, permutation testing was used, where the correspondence between behavioral variables and connectivity matrices were randomly shuffled 1,000 times and the CPM analysis was re-run with the shuffled data to generate null distributions of $\sqrt{R_{CV}^2}$. Based on these null distributions, the p-values for predictions were calculated as: p=(#[ρ_null>ρ_median]+1)/1001, where #[ρ_null>ρ_median] indicates the number of permutated predictions numerically greater than the median of the un-permutated predictions. As only a positive association between predicted and actual values can indicate prediction above chance levels, one-tailed p-values are reported. In other

words, negative associations (even large effect size) indicate a failure to predict and accordingly are not tested for significance.

Virtual lesion analysis

CPM predictive networks are typically widespread and complex, so we conducted a virtual lesion analysis. For a CPM-based virtual lesion analysis, predictive networks can be set to zero to examine the degradation in predictive performance attributed to a virtual lesion of that network (11, 12). We conducted two versions of virtual lesion analysis. First, we iteratively set each functional network to zero and examined how this impacted the model performance. We conducted this virtual lesion analysis for the canonical functional networks: medial frontal (MF), frontoparietal (FP), default mode (DMN), motor (MOT), visual I (VI), visual II (VII), visual association (VA), salience (SAL), subcortical (SC), and cerebellum (CBL). Second, we analyzed with only leaving the connectivity values "unlesioned" for each network and setting the rest of the connectivity matrix to zero to examine the predictive performance of each network in isolation.

Quantification of task and anatomical contribution to prediction

Predictive networks identified using CPM are complex and composed of multiple brain regions and networks. To quantify the contribution of each edge to a given predictive model, we calculated the k^{th} edge's weight for m^{th} task (labeled $W_{k,m}$) to the model as: $W_{k,m} = \boldsymbol{B}(k,m)abs({\beta_m}^k)std(\boldsymbol{E}_k(:,m))$, where $\boldsymbol{B}(k,m)$indexes whether the k^{th} edge is selected from the m^{th} task, $std(\boldsymbol{E}_k(:,m))$ represents the standard deviation of the k^{th} edge in the m^{th} task, and ${\beta_m}^k$ represents the weight learned by CPM for the k^{th} edge in the m^{th} task. To quantify the contribution of each node to a given predictive

model, we calculated the n^{th} node's weight summed across all tasks and edges (labeled W_n) to the model as: $W_n = \sum_{k=1}^{35,778} \sum_{m=1}^{3} W_{k,m}$, for all k edges connected to the n^{th} node. Next, for the network level, $W_{k,m}$ was averaged over each edge within or between canonical functional networks, based on the functional networks presented in (13). Finally, we quantified the contribution of each task as: $W_n = \sum_{k=1}^{35,778} W_{k,m}$. To increase interpretablility, W_m are then normalized to have sum of 1, $\sum_{m=1}^{3} W_m = 1$, so that it represents each task's proportional contribution in the model.

Anatomical localization of group differences in connectomes

To measure group differences in task connectomes (i.e., appetitive, stress, neutral-relaxing connectomes) between the substance use-related and control groups, mass univariate, edge-wise analyses was used, and multiple comparisons were controlled using the Network-Based Statistic (NBS) (14). For each edge, connectivity strength from each task-based connectome is included in a two-tailed t-test resulting in a node-by-node matrix of t-values that represent the magnitude of differences across groups. This procedure was performed independently for each task-based connectome. One-thousand iterations and an initial t-value threshold of 2.595 were used for NBS. Results at p<0.0167 (0.05/3) were considered significant. For the comparisons with the predictive modeling results, node contributions were quantified at the sum of all significant edges for a node. Edges showing greater and weaker connectivity between groups were summarized independently. In addition, results were also summarized across all task connectomes by creating the union of all significant edges from each task connectome, and summarizing node contribution as above.

Model overlap

To assess the overlap between the transdiagnostic, predictive model of craving and group differences in connectomes, the node-level contributions were correlated between predictive models and group difference results.

Code and model availability

Matlab scripts to run the main CPM analyses can be found at https://github.com/YaleMRRC/CPM/tree/master/matlab/func/misc. BioImage Suite tools used for analysis and visualization can be accessed at www.bisweb.yale.edu. Models are shared at https://www.nitrc.org/projects/bioimagesuite/.

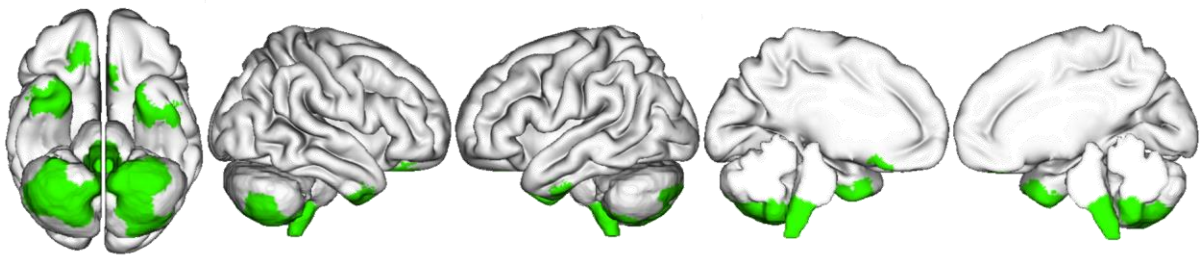

FIGURE S1. Spatial location of nodes removed from analysis due to incomplete slice coverage across subjects (green). These twenty-one nodes were located in the brain stem, inferior cerebellum, temporal pole, and inferior orbital frontal lobe. These nodes were primarily in the cerebellum and brain stem.

Supplementary Results

Self-reported craving

Craving ratings for the substance use-related group and the control group are presented in Table S1. For all conditions, the substance use-related group reported higher craving compared to the control group (appetitive: $t=3.32$, $p=0.001$, $df= 296.17$; stress: $t=4.00$, $p<0.001$, $df= 293.07$; neutral-relaxing: $t=3.49$, $p<0.001$, $df= 278.71$). In the appetitive and stress conditions, craving ratings after the task were greater than craving ratings before the task (appetitive: $t=6.00$, $p<0.001$, $df= 257.05$; stress: $t=2.65$, $p=0.009$, $df=261.81$). There were no significant group-by-time interactions. All models included gender and age as covariates. Craving ratings from the substance use-related group exhibited greater variance than craving ratings from the control group (Bartlett $c^2= 53.3$, $p<0.001$, $df=3$). Craving ratings were highly correlated within and across imagery conditions ($r's>0.86$, $p's<0.001$, $df=272$). These correlations were similar for the substance use-related ($r's>0.85$, $p's<0.001$, $df=124$) and control groups ($r's>0.86$, $p's<0.001$, $df=146$), independently. Finally, the alpha reliability of craving response within subjects and across participants was $\alpha = .9835$.

Alternative models

Potential differences in prediction performance between craving rated before and after the imagery conditions were tested (Table S2). Notably, prediction of craving measured before the imagery conditions was significantly better than prediction of craving measured after the imagery conditions when using either the 1st principal component ($z=3.43$, $p<0.001$) or the mean craving ($z=2.14$, $p=0.032$).

We investigated whether the multidimensional approach of combining connectomes and craving ratings from multiple imagery conditions produced better predictions over using a single imagery condition and craving rating (Table S3). In all cases, prediction using a single imagery condition and craving rating was significantly worse than the multidimensional model (appetitive: $z=10.85$, $p<0.001$; stress: $z=10.59$, $p<0.001$; neutral-relaxing: $z=4.50$, $p<0.001$).

Finally, instead of using each task connectome as features for prediction, we simply averaged the three connectomes together results in a single connectome per participant. Prediction performance remained high, but worse than our original model.

Prediction residuals for each group

In a post-hoc manner, we explored if there were any group differences in the residuals of prediction performance (i.e., whether prediction was driven by one group over the other). The control group compared to the substance use-related group showed lower r, ρ, and q^2 but also a lower mean square error (MSE) (control group: $r=0.25$, $\rho=0.15$, $q^2=0.06$, MSE=28.65; substance use-related group: $r=0.52$, $\rho=0.56$, $q^2=0.20$, MSE=39.87). Overall, these differences are in line with the group differences in spread and mean of the craving values (Table S1). The control group has less variance in craving, which will lead to a smaller correlation between predicted and observed craving, and lower mean craving, which will lead to a smaller mean square error. Regardless of these numerical differences, predictions are strong in each group.

Predictions without performing global signal regression

As there is the potential for widespread activation from neural response to drug cues, which might contaminate the global signal, we repeated the main analyses

without performing global signal regression. Overall, prediction results were similar (r=0.35, ρ=0.40, q^2=0.15, MSE=33.67), suggesting that group differences in global signal were not driving the prediction performance.

Gender-related differences in predictions of craving

Based on putative sex/gender differences in the neural substrates of craving (e.g., 3), we investigated whether gender moderated the prediction of craving. The CPM analysis was repeated in each gender independently. Prediction performance was numerically higher but not significantly different in women compared to men (women: r=0.38, ρ=0.35, q^2=0.13, MSE=34.93, n=178; men: r=0.20, ρ=0.20, q^2=0.04, MSE=38.00, n=96; z=1.54, p=0.12). Likewise, models trained only in women predicted craving in men (r=0.39, p<0.001, df=176) and vice versa (r=0.43, p<0.001, df=94).

Virtual lesion analysis

First, we excluded only individual networks from CPM (e.g. predictions were preformed using all networks except the DMN). In all cases, predictions removing any single network were still significant (p's<0.01), suggesting that no single network is responsible for prediction. As shown in Table S5, when excluding a single network, subcortical, salience, and default mode networks produced the largest reductions in prediction performance, suggesting these networks contribute the most towards prediction. Next, we ran CPM using edges from only a single network. Using a single network for prediction resulted in significant predictions for all networks (p's<0.01). As shown in Table S6, the subcortical, salience, and default mode networks showed the best single networks for prediction, in alignment with the findings above. The cerebellum network produced the worst prediction performance of all networks, although this might

be confounded by the large number of missing nodes in this network (Figure S1). Finally, using a linear search, the best combination of networks for prediction was found using the subcortical, salience, and default mode networks, which performed numerically (but not significantly) better than the next two best performing combinations (all networks and subcortical plus salience networks).

Group differences in connectivity

Across all conditions, 1547 edges, or about 5% of the total number of possible edges, exhibited significant ($p<0.05$, corrected) group differences in connectivity between the substance use-related and control groups (Figure S4). Overall, the nodes contributing to prediction and the nodes contributing to group differences were not correlated, suggesting that the predictive modeling results are neurobiologically distinct from the group differences (all conditions: $r=-0.07$, $p=0.25$, $df=245$; appetitive: $r=-0.021$, $p=0.75$, $df=245$; stress: $r=0.01$, $p=0.92$, $df=245$; neutral-relaxing: $r=-0.021$, $p=0.75$, $df=245$). The nodes with the largest number of significant edges that differed between groups were located in the cerebellum, brainstem, PCC, and frontoparietal association cortices (Figure S4). When considering these edges across conditions, stronger connectivity during the appetitive condition, and both stronger and weaker connectivity during the stress condition (i.e., for different edges), for the substance use-related group compared to control group, contributed most of these edges (691, 421, 410, respectively). In general, the group differences in cerebellar and brainstem edges were observed during the appetitive condition, while the group differences in the PCC and association cortices were observed during the stress condition. No significant group differences during the neutral-relaxing condition were observed.

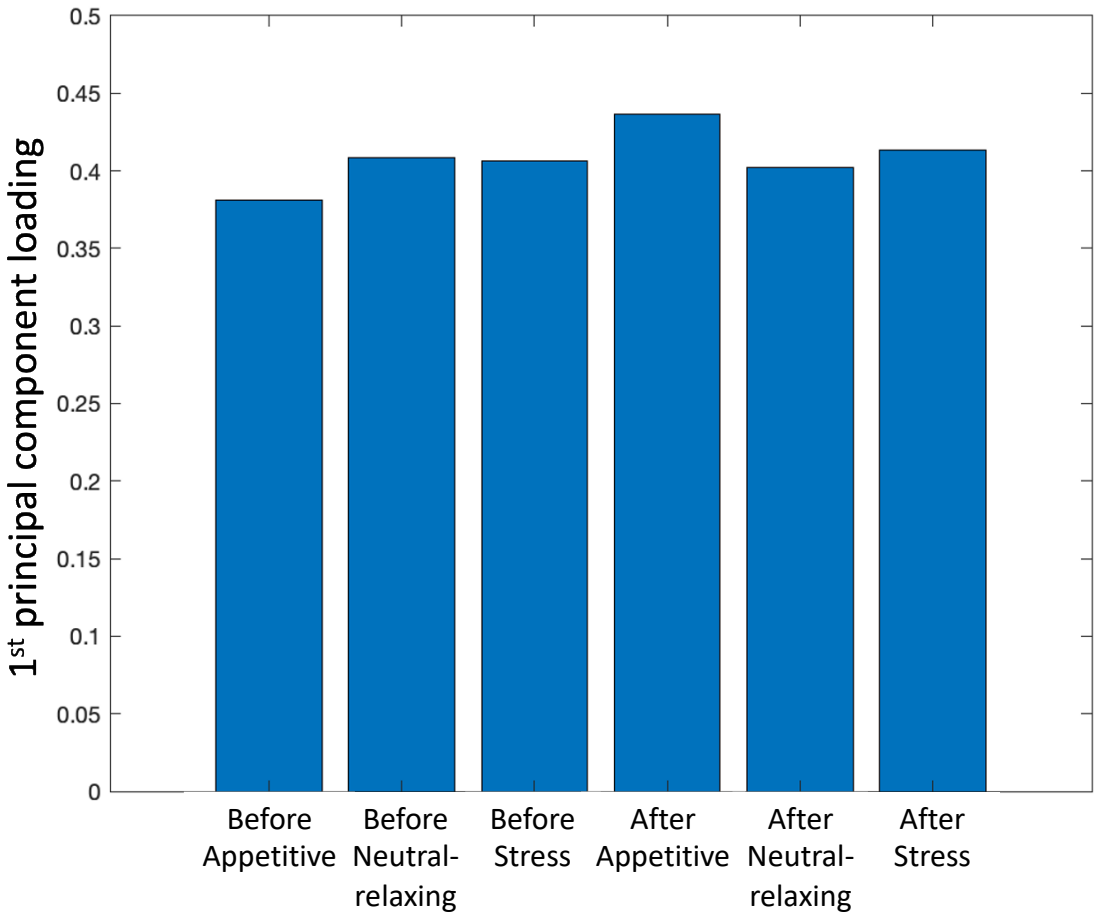

FIGURE S2. Loadings of the 1st principal component across all craving measures. Across 6 self-report craving measures taken before and after each imagery condition, each craving measure contributed approximately equally to the 1st principal component used in prediction.

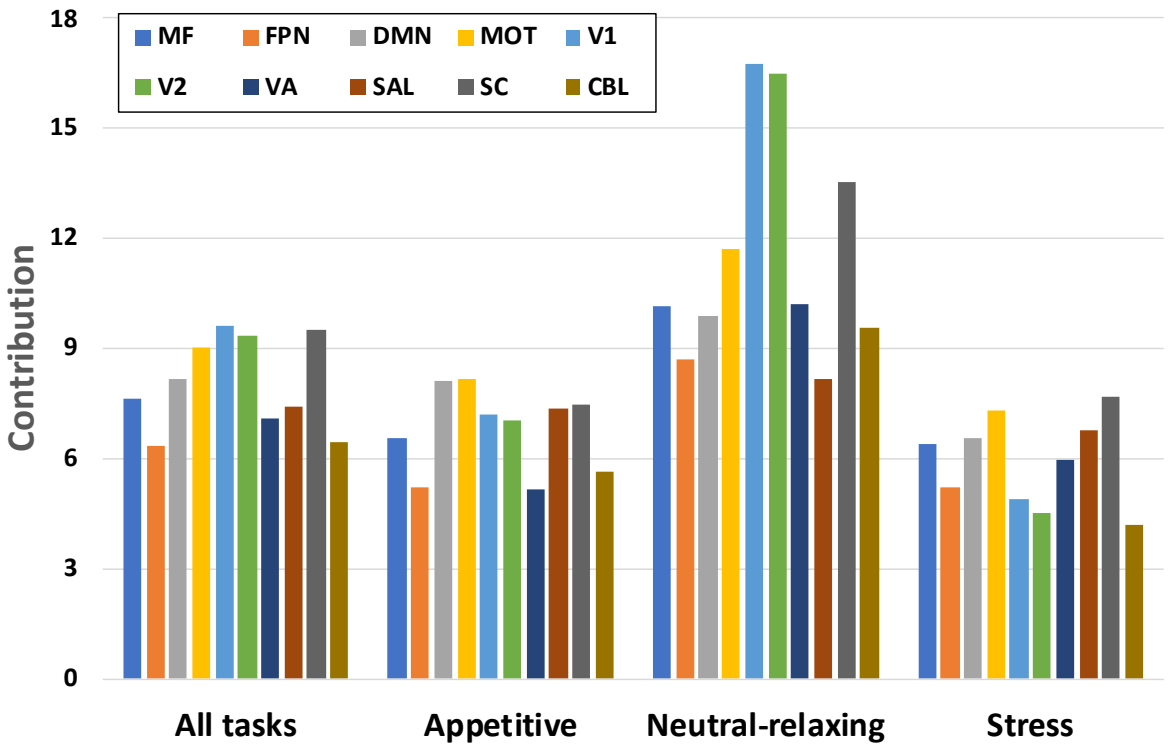

FIGURE S3. Total network-level contribution to predicted craving. Plotted values were calculated by sum over each each row (or column) in Figure 4 to produce a single summary number for total network-level contribution. For the appetive condition, the DMN and motor-sensory network contributed the most. For the neutral-relaxing condition, the visual networks contributed the most. For the stress condition, the subcortical and motor-sensory networks contributed the most. Missing nodes were primarly in the cerebellar network, which may impact the contribution of this network. MF=medial frontal network; FPN=frontal parietal network; MOT=motor-sensory network; V1=visual network #1; V2=visual network #2; VA=visual association network; SAL=salience network; SC=subcortical network; CBL=cerebellar network.

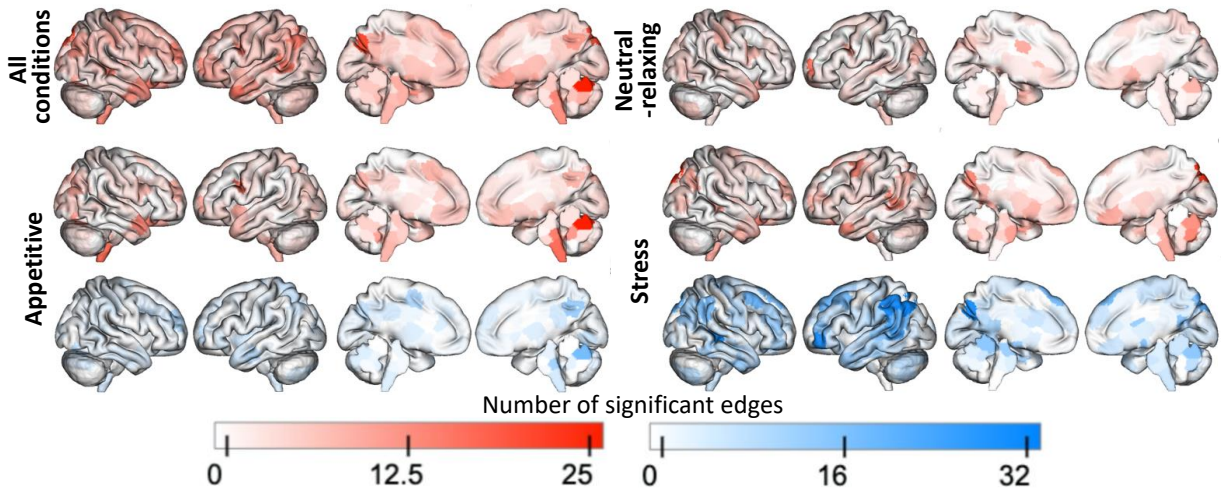

FIGURE S4. Node-level contribution to group differences in connectivity. One-thousand-five-hundred-and-forty-seven edges, or about 5% of the total number of possible edges, exhibited significant ($p<0.05$, corrected) group differences in connectivity between the substance use-related and control groups. The nodes with the largest number of significant edges that differed between groups were located in the cerebellum, brainstem, PCC, and frontoparietal association cortices. Overall, the nodes contributing to prediction and the nodes contributing to the group differences were different and not overlapping. Warmer regions (darker red) indicate either regions of largest number of significant edges that differed between groups (All conditions) or regions of largest number of significant edges that were greater in the substance use-related group compared to the control group (Appetite, Neutral-relaxing, Stress). Cooler regions (darker blue) indicate regions of largest number of significant edges that were weaker in the substance use-related group compared to the control group.

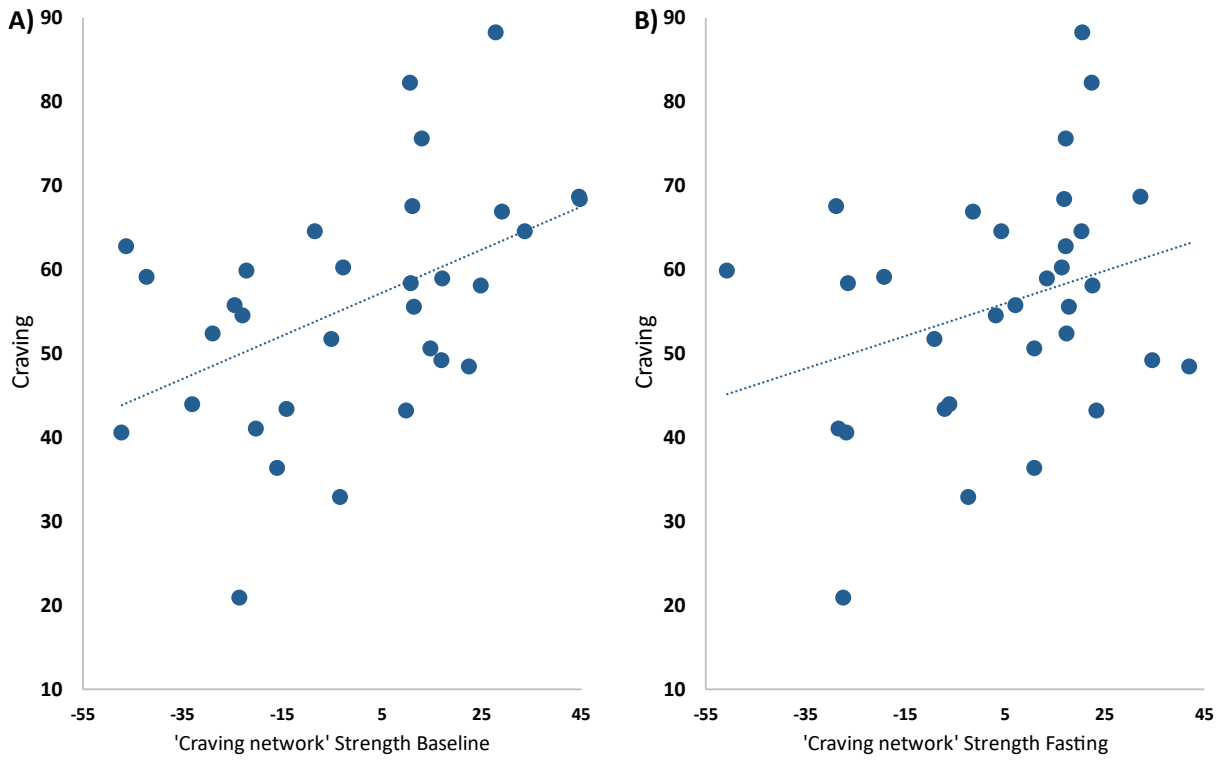

FIGURE S5. Scatter plots for the external validation sample. In an independent set of individuals collected using a different fMRI task paradigm and measures of self-reported craving, the 'craving network' successfully predicted self-reported craving of food during 10 hours of fasting using both the baseline scans (r=0.47, p=0.003, df=30) and after fasting scans (r=0.31, p=0.04, df=30). The difference in prediction performance using baseline and fasting scans was not significant (z=1.01, p=0.31, Steiger's test).

TABLE S1. Self-reported craving. Craving data are presented as means with standard deviations in parentheses.

Group	Before appetite condition	After appetite condition	Before neutral-relaxing condition	After neutral-relaxing condition	Before stress condition	After stress condition
Total Sample	1.44 (2.48)	2.24 (2.92)	1.63 (2.66)	1.53 (2.63)	1.62 (2.65)	1.82 (2.75)
Controls	0.96 (1.92)	1.68 (2.37)	1.07 (2.02)	0.95 (1.97)	1.04 (1.95)	1.17 (1.99)
Substance use-related disorders	1.88 (2.82)	2.74 (3.27)	2.12 (3.04)	2.04 (3.02)	2.14 (3.05)	2.39 (3.18)

TABLE S2. Prediction performance using mean craving compared to PCA

Variable	r	ρ	q^2	MSE	p-value
Mean craving across all conditions	0.41	0.38	0.14	3.37	p<0.001
Mean craving before all conditions	0.44	0.44	0.16	2.87	p<0.001
Mean craving after all conditions	0.38	0.36	0.13	3.88	p<0.001
PCA on craving before all conditions	0.45	0.45	0.17	16.37	p<0.001
PCA on craving after all conditions	0.37	0.34	0.12	18.65	p<0.001

Pearson's correlation (r), Spearman's rank correlation (ρ), cross-validated coefficient of determination (q^2), and mean square error (MSE) between observed and predicted values

TABLE S3. Prediction performance using a single imagery condition

Task	r	ρ	q^2	MSE	p-value
Appetitive imagery alone	0.29	0.28	0.06	3.57	p<0.001
Neutral-relaxing imagery alone	0.36	0.35	0.1	2.78	p<0.001
Stress imagery alone	0.29	0.34	0.05	3.07	p<0.001

Pearson's correlation (r), Spearman's rank correlation (r), cross-validated coefficient of determination (q^2), and mean square error (MSE) between observed and predicted values

TABLE S4. Prediction from differences between task connectomes

Contrast	r	ρ	q^2	MSE	p-value
Appetitive – Neutral-relaxing	-0.03	-0.01	0.0	0	1
Neutral-relaxing – Stress	-0.04	0.01	0.0	0	1
Appetitive – Stress	0.04	0.08	0.07	9.6	.82

TABLE S5. Change in prediction performance after excluding a single network

Excluded network	r	P value	% change
Subcortical	0.35	<0.001	-5.79
Salience	0.35	<0.001	-5.58
Default Mode	0.36	<0.001	-3.86
Sensory-Motor	0.36	<0.001	-2.92
Medial Frontal	0.37	<0.001	-1.29
Visual Association	0.38	<0.001	1.07
Visual II	0.38	<0.001	1.42
Visual I	0.38	<0.001	2.28
Frontoparietal	0.38	<0.001	2.82
Cerebellar	0.38	<0.001	2.95

TABLE S6. Change in prediction including only a single network

Included network	r	P value	% change
Subcortical	0.38	<0.001	1.90
Salience	0.36	<0.001	-2.15
Default Mode	0.34	<0.001	-7.99
Sensory-Motor	0.34	<0.001	-8.93
Medial Frontal	0.32	<0.001	-15.29
Visual Association	0.27	<0.001	-28.7
Visual II	0.26	<0.001	-31.2
Visual I	0.24	<0.001	-35.19
Frontoparietal	0.21	<0.001	-43.51
Cerebellar	0.17	0.01	-54.91

Supplementary References

1. Hommer RE, Seo D, Lacadie CM, Chaplin TM, Mayes LC, Sinha R, Potenza MN. Neural correlates of stress and favorite-food cue exposure in adolescents: a functional magnetic resonance imaging study. Hum Brain Mapp. 2013;34:2561-2573.
2. Jastreboff AM, Sinha R, Lacadie C, Small DM, Sherwin RS, Potenza MN. Neural correlates of stress- and food cue-induced food craving in obesity: association with insulin levels. Diabetes Care. 2013;36:394-402.
3. Potenza MN, Hong KI, Lacadie CM, Fulbright RK, Tuit KL, Sinha R. Neural correlates of stress-induced and cue-induced drug craving: influences of sex and cocaine dependence. Am J Psychiatry. 2012;169:406-414.
4. Seo D, Jia Z, Lacadie CM, Tsou KA, Bergquist K, Sinha R. Sex differences in neural responses to stress and alcohol context cues. Hum Brain Mapp. 2011;32:1998-2013.
5. Seo D, Lacadie CM, Tuit K, Hong KI, Constable RT, Sinha R. Disrupted ventromedial prefrontal function, alcohol craving, and subsequent relapse risk. JAMA Psychiatry. 2013;70:727-739.
6. Yip SW, Lacadie CM, Sinha R, Mayes LC, Potenza MN. Prenatal cocaine exposure, illicit-substance use and stress and craving processes during adolescence. Drug Alcohol Depend. 2016;158:76-85.
7. Yip S, Potenza E, Balodis IM, Lacadie C, Sinha R, Mayes L, Potenza MN. Prenatal cocaine exposure and adolescent neural responses to appetitive and stressful stimuli. Neuropsychopharmacol. 2014;39:2824-2834.
8. Joshi A, Scheinost D, Okuda H, Belhachemi D, Murphy I, Staib LH, Papademetris X. Unified framework for development, deployment and robust testing of neuroimaging algorithms. Neuroinformatics. 2011;9:69-84.
9. Shen X, Finn E, Scheinost D, Rosenberg M, Chun M, Papademetris X, Constable R. Using connectomebased predictive modeling to predict individual behavior from brain connectivity. nature protocols. 2017 Mar; 12 (3): 506.

10. Scheinost D, Kwon SH, Lacadie C, Vohr BR, Schneider KC, Papademetris X, Constable RT, Ment LR. Alterations in Anatomical Covariance in the Prematurely Born. Cerebral Cortex. 2017;27:534-543.
11. Yip SW, Kiluk B, Scheinost D. Toward addiction prediction: an overview of cross-validated predictive modeling findings and considerations for future neuroimaging research. Biological Psychiatry: Cognitive Neuroscience and Neuroimaging. 2020;5:748-758.
12. Ibrahim K, Noble S, He G, Lacadie C, Crowley MJ, McCarthy G, Scheinost D, Sukhodolsky DG. Large-scale functional brain networks of maladaptive childhood aggression identified by connectome-based predictive modeling. Mol Psychiatry. 2022 Feb; 27(2):985-999.
13. Noble S, Scheinost D, Finn ES, Shen X, Papademetris X, McEwen SC, Bearden CE, Addington J, Goodyear B, Cadenhead KS, Mirzakhanian H, Cornblatt BA, Olvet DM, Mathalon DH, McGlashan TH, Perkins DO, Belger A, Seidman LJ, Thermenos H, Tsuang MT, van Erp TG, Walker EF, Hamann S, Woods SW, Cannon TD, Constable RT. Multisite reliability of MR-based functional connectivity. Neuroimage. 2017;146:959-970.
14. Zalesky A, Fornito A, Bullmore ET. Network-based statistic: identifying differences in brain networks. Neuroimage. 2010;53:1197-1207.